Superconducting critical fields of alkali and alkaline-earth intercalates of MoS_2

John A. Woollam
NASA Lewis Research Center, Cleveland, Ohio 44135

Robert B. Somoano
Jet Propulsion Laboratory, Pasadena, California 91103
(Received 30 June 1975)

The critical-field anisotropy and temperature dependence of the alkali and alkaline-earth intercalates of MoS_2 have been measured. There are three principal results: First, an unusual positive curvature in the critical-field-temperature boundary has been observed. This curvature appears to be a universal feature of layered superconductors and possible theoretical explanations are discussed. Secondly, the critical-field anisotropy is compared with two models, a coupled-layer model and an uncoupled-layer or thin-film model. Which model fits the data depends on the material, and it is apparent that very accurate experimental data must be taken to distinguish between the models. Our third principal result is the grouping of properties of the alkali and alkaline-earth series of intercalates. The materials with the largest ionic intercalate atom diameters and hexagonal structures (K, Rb, and Cs compounds) have the highest critical temperatures, critical fields, and critical boundary slopes. In all cases the hexagonal materials have critical fields exceeding the paramagnetic limiting fields. The second group, consisting of the nonhexagonal Na, Sr, and Ca intercalates, have lower critical temperatures and fields, and the paramagnetic limit is not exceeded.

I. INTRODUCTION

The transition-metal dichalcogenides of groups IV*B*, V*B*, and VI*B* exhibit considerable diversity in their physical properties, spanning the fields of metals, semiconductors, insulators, and superconductors.[1] An important feature of these materials is that they crystallize in layered structures which imparts substantial anisotropy to many of their properties. In addition, the layered structure facilitates the process of "intercalation," or insertion of foreign atoms and molecules into these materials, thus allowing a convenient method for altering the structure and electronic behavior.[2] In this paper, we discuss the critical-field properties of the group-VI*B* semiconductor molybdenum disulfide MoS_2 intercalated with alkali and alkaline-earth metals.

Molybdenum disulfide is a layered diamagnetic semiconductor (Fig. 1). Within each layer, there exists trigonal prismatic coordination between the Mo and S atoms and the bonding is primarily covalent. The stacking sequence of the layers can result in the formation of either a hexagonal (2*H*) or rhombohedral (3*R*) polymorph. The bonding between the layers is due to weak Van der Waals forces, and it is this weak interaction that allows the acceptance of alkali or alkaline-earth atoms or ions into the interlayer gap.

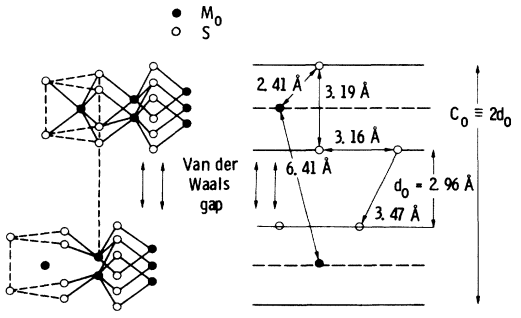

FIG. 1. Structure of MoS_2.

The reaction of alkali and alkaline-earth metals dissolved in liquid ammonia with MoS_2 results in a series of metallic superconducting intercalation compounds.[3-6] The metal penetrates between the semiconducting layers and donates at least part of its electron to MoS_2, with the resulting intercalation compound being metallic. The alkali and alkaline-earth intercalates, A_xMoS_2 (A = Na, K, Rb, Cs, Ca, and Sr) can be separated into two groups according to their stoichiometry, structure, and superconducting properties (see Tables I and II). The first group consists of the Na, Ca, and Sr intercalates which have nonhexagonal structures, less well-defined stoichiometries, small intercalate ion diameters, superconduct at temperatures of 3.6, 4.0, and 5.6 °K, respectively, and have similar critical properties. The uncertainties in the stoichiometry of the compounds in this group are Na_xMoS_2 ($0.3 \leq x \leq 0.6$), Ca_xMoS_2 ($0.05 \leq x \leq 0.07$), and Sr_xMoS_2 ($0.06 \leq x \leq 0.1$). The second group consists of the K, Rb, and Cs intercalates which form compounds of definite stoichiometry ($x \simeq 0.3$), have a well-ordered hexagonal crystal structure, larger intercalate ion diameters, superconduct at $T = 6.9$ °K, and show similarities in their critical properties.

The lithium intercalate Li_xMoS_2 also has a less

TABLE I. Crystal structure, ionic diameter, ionization potential, and transition temperature of the alkali and alkaline-earth intercalates of MoS_2 listed in order of increasing ionic diameters (Ref. 4 and 6).

Compound	Crystal structure	Ionic diameter (Å)		Ionization potential (eV)	T_c
Na_xMoS_2 $(0.3 \leq x \leq 0.6)$	Tetragonal	Na^{1+}	1.94	5.14	3.6
Ca_xMoS_2 $(0.05 \leq x \leq 0.07)$	Orthorhombic	Ca^{2+}	1.98	6.11	4.0
Sr_xMoS_2 $(0.06 \leq x \leq 0.1)$	Tetragonal	Sr^{2+}	2.24	5.69	5.6
$K_{0.4}MoS_2$	Hexagonal	K^{1+}	2.66	4.34	6.9
$Rb_{0.3}MoS_2$		Rb^{1+}	2.94	4.18	6.9
$Cs_{0.3}MoS_2$		Cs^{1+}	3.34	3.89	6.9
MoS_2 $(2H)$	Hexagonal	Mo^{4+}	1.40		
		Mo [a]	2.74		
		Mo–S [b]	2.41		None

[a] Covalent diameter.
[b] Mo–S distance in $(2H)$ MoS_2.

well defined stoichiometry and superconducts at 3.7 °K. However, it differs from the compounds mentioned above in that NH_3 or NH_2 intercalates along with Li, and the resulting structure exhibits considerable disorder (i.e., loss of horizontal registry) that prevents an adequate x-ray structure determination.

The transport properties of MoS_2 are quite anisotropic owing to the layered structure, and similar anisotropies are observed in other layered transition-metal dichalcogenides. The critical-field properties of superconducting layered transition-metal dichalcogenides, such as TaS_2, $(TaS_2)(C_5H_5N)_{1/2}$, and $NbSe_2$, have been measured and they reveal considerable anisotropy.[7-9]

The purpose of this paper is to describe the temperature dependence and anisotropy of the critical fields, $B_{c2}(\theta, T) \equiv \mu H_{c2}(\theta, T)$ of A_xMoS_2 (where A = Na, K, Rb, Cs, Ca, and Sr), and to compare trends throughout the series of intercalates. The temperature dependences are compared with present theories for B_{c2} vs T_c in the clean and dirty limit, and over the range of reduced temperature ($t = T/T_c$) from 1 to 0.1. Critical-field boundaries are found to be steep in all cases, with B_{c2} being greater than theoretical predictions at low temperatures. Secondly, an unusual positive curvature in the temperature de-

TABLE II. Data for alkali and alkaline-earth intercalates of MoS_2, as well as for three other layered superconductors (Ref. 8). Comparison of transition temperature, T_c; low-temperature limit for positive curvature, t^*; critical fields at $T=0$, $B_{c2\parallel}(0)$, $B_{c2\perp}(0)$; paramagnetic limiting field, $B_p = 1.84\ T_c$; critical-field ratios; and critical field vs critical temperature negative slopes. 1T = 10 kG.

Compound	T_c (°K)	t^* [a]	$B_{c2\parallel}(0)$ [a] (tesla)	B_p (tesla)	$B_{c2\perp}(0)$ [b] (tesla)	$B_{c2\parallel}(0)/B_{c2\perp}(0)$ [b]	$B_{c2\parallel}(0)/B_{c2\perp}(0)$ [c]	$-dB_{c2\parallel}/dT_c$ [d] (tesla/K)	$-dB_{c2\perp}/dT_c$ [d] (tesla/K)
Na_xMoS_2	3.6	0.7	5	6.6	0.76	6.6	6.7	2	0.3
Ca_xMoS_2	4.0	0.5	2.1	7.4	0.65	3.2	$\gtrsim 5$	1.8	0.3
Sr_xMoS_2	5.6	0.7	4.6	10.3	1.36	3.4	$\gtrsim 4$	1.6	0.3
$K_{0.4}MoS_2$	6.9	0.9	···	12.7	4	···	···	4	0.7
$Rb_{0.3}MoS_2$	6.9	0.9	···	12.7	4	···	···	3	0.8
$Cs_{0.3}MoS_2$	6.9	0.8	22	12.7	3.3	6.7	6.1	5	0.6
$NbSe_2$	7.3	0.9	14	13.4	4.0	3.5	3.5	3	0.7
$TaS_2(C_5H_5N)$ [e]	3.6	0.8	>25	6.6	···	···	···	7	0.4
TaS_1Se_1 [e]	3.6	0.7	16	6.6	2.5	6.4	5.8	5	0.9

[a] $B_{c2\parallel}$ data only. Numbers valid to within ±10%.
[b] Estimated by extrapolating to 0 °K from lowest temperature experimental point, using Eq. (1) of text. This equation gives values generally too low, but does give a rough estimate.
[c] From experimental data linearly extrapolated to $T=0$.
[d] Evaluated at $t < t^*$.
[e] From Ref. 8.

pendence of B_{c2} is observed which may be related to the high anisotropy of the layer structure.[10]

The critical-field anisotropy data $B_{c2}(\theta)$ are compared with predictions based on a coupled layers model, as well as with a thin-film, or "independent layers," model. Computer plots of the predictions of these models show that very accurate data must be taken to distinguish the better fit between models, especially for the most highly anisotropic materials. The major differences between the models occur when the field is within 20° of being parallel to the layer planes.

II. EXPERIMENTAL

The alkali and alkaline-earth intercalates were prepared and characterized according to procedures described elsewhere.[3,4,6]

Critical-field studies were carried out on all of the alkali-metal intercalates except Li_xMoS_2. Since the critical-field properties of the K, Rb, and Cs intercalates were quite similar, a detailed examination was only made on $Cs_{0.3}MoS_2$. For comparative purposes, low-field properties of $NbSe_2$ were measured near T_c on a single crystal grown by chemical vapor transport, using iodine as the carrier gas.

Critical-field data were taken in fields up to 11 Tesla and temperatures down to 1.1°K. Two magnets were used, one providing up to 3.5 Tesla in a split pair with horizontal access, the other providing 11 Tesla in a solenoidal geometry. In the 3.5-Tesla magnet, the angle between the magnetic field and the crystal-layer planes could be controlled to within 0.2°, and in the 11-Tesla magnet the angle could be determined to within 0.3°. Field strengths were measured by Hall-effect devices and magnetoresistors calibrated by nuclear resonance at various fields to about 8 Tesla.

Sample temperatures were monitored with carbon thermometers calibrated initially in liquid nitrogen, hydrogen, and pumped helium with corrections for thermometer magnetoresistance. Before or after each run, thermometers were recalibrated against helium vapor pressure below 4.2°K. Periodic checks were made by calibrating against a germanium thermometer above 4°K (in zero magnetic field) and by checking the T_c of lead and $NbSe_2$.

The superconducting transition temperature was taken as the temperature for the onset of diamagnetism, as measured by a modified Schawlow-Devlin self-inductance method.[11] Most data were taken by fixing the angle θ between the magnetic field and the layer planes and subsequently raising the temperature through the transition. Data were also taken by fixing the field and temperature, and then rotating the sample to an angle where B_{c2} was greater than the applied field, at which point the sample suddenly became diamagnetic. The angles for the onset of diamagnetism could then be plotted for a series of magnetic field strengths to give plots of B_{c2} vs θ at fixed T. This was found to be an accurate and rapid method of determining the angular dependence of B_{c2}.

III. RESULTS

A. Temperature dependence of B_{c2}

The temperature dependence of B_{c2} for Na_xMoS_2 with the field oriented parallel ($B_{c2\parallel}$) and perpendicular ($B_{c2\perp}$) to the layers is shown in Fig. 2 and similar data for Ca_x, Sr_x, and $Cs_{0.3}MoS_2$ are shown in Figs. 3–5. We observed similar critical field data in $NbSe_2$. Shown in the inset is $m_\perp/m_\parallel = (B_{c2\parallel}/B_{c2\perp})^2$ as a function of temperature as de-

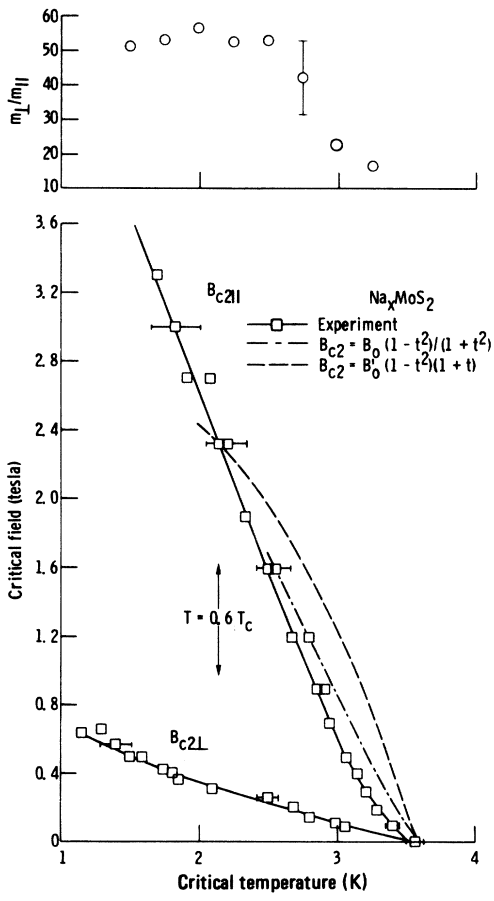

FIG. 2. $B_{c2\parallel}$ and $B_{c2\perp}$ vs T_c for Na_xMoS_2. Critical temperature is taken as the temperature for the onset of diamagnetism. Shown are plots of Eqs. (1) and (2) when clarity allows. Inset is $m_\perp/m_\parallel = (B_{c2\parallel}/B_{c2\perp})^2$ as a function of temperature [Eq. (11)] found from best fits through the B_{c2} vs T_c data.

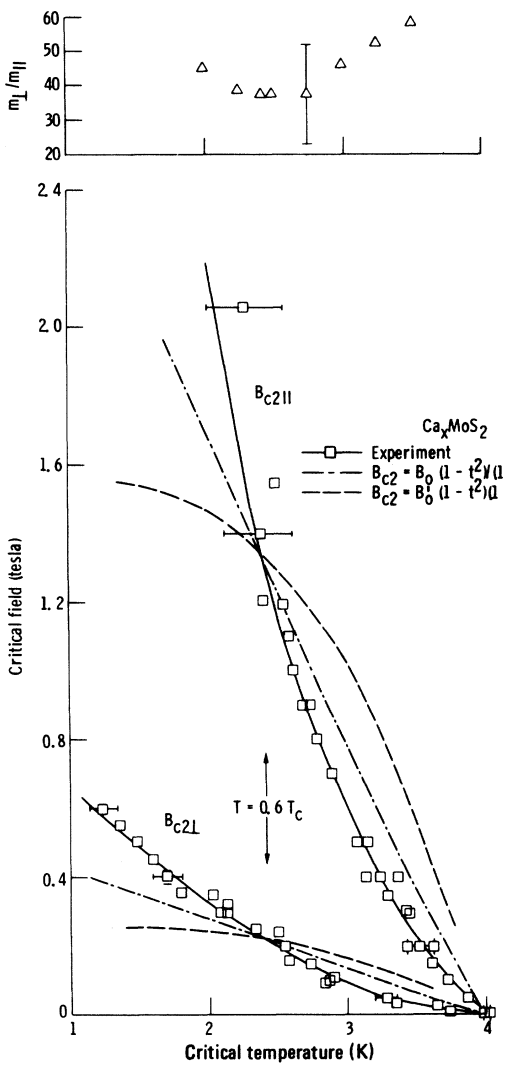

FIG. 3. Same as Fig. 2 for Ca_xMoS_2.

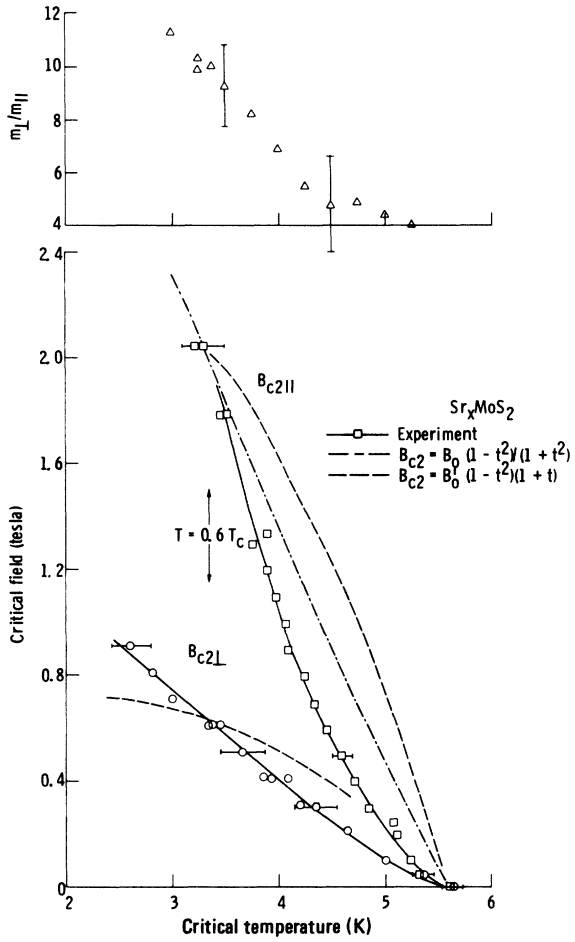

FIG. 4. Same as Fig. 2 for Sr_xMoS_2.

termined from best fits through the B_{c2} vs T_c data and using Eq. (11). A summary of data is given in Table II. An unusual and interesting feature is the positive curvatures (PC) of the critical-field boundaries for temperatures near the zero-field onset temperature T_c for both orientations. The greatest amount of PC occurs for the parallel orientation, and decreases as the angle θ between the applied field and the layers approaches 90° (perpendicular orientation). The curvature occurs over a wide range of reduced temperatures t ($t \equiv T/T_c$). The range is between $t = t^*$ and $t = 1$ for all compounds, where t^* is defined as the reduced temperature above which positive curvature exists. It is difficult to determine t^* precisely from the data, but estimates have been made (see Table II) and indicate that the Ca compound has the widest temperature range of positive curvature. There is no clear trend in the degree of PC, within experimental error, in the K, Rb, and Cs intercalation group, but curvature for this group tends to be greater than for the Na, Ca, and Sr group.

As shown in a previous publication,[10] the temperature dependence of $B_{c2\parallel}$ and $B_{c2\perp}$ cannot be accounted for by any simple power law. This is particularly true for the region of PC. In the temperature range below the PC region, an equation based on the Gorter-Casimir two-fluid model

$$B_{c2}(t) = B_{c2}(0)[(1-t^2)/(1+t^2)] \quad (1)$$

comes closest of all theories tested to approximating the data. Plots of Eq. (1) are shown in Figs. 2–5, fitted to the data at the crossover point $t = 0.6$. It should be stressed that Eq. (1) does not fit the data, but is used for comparative purposes only. Values of $B_{c2}(0)$ (the zero-temperature critical field) were determined by linear extrapolation of the data to $t = 0$, as well as by extrapolation of Eq. (1) fit to the lowest-temperature–highest-

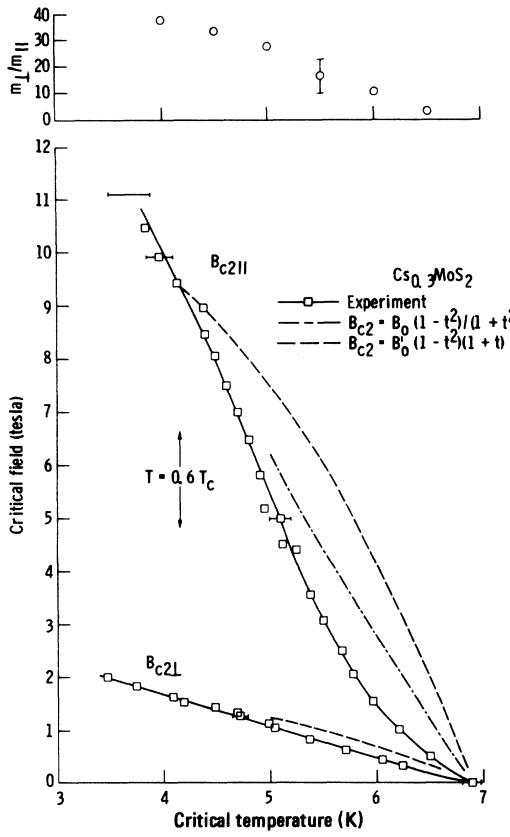

FIG. 5. Same as Fig. 2 for $Cs_{0.3}MoS_2$.

field experimental points. Both of these methods are used to compute numbers in Table II. Also shown in Table II are the critical field slopes, $dB_{c2\parallel,\perp}/dT$, evaluated in the temperature region just below the PC. The fit of Eq. (1) is better for Na_xMoS_2 (particularly for $B_{c2\perp}$) than for the other compounds, and therefore, the values for $B_{c2\parallel,\perp}(0)$ shown in Table II for Na_xMoS_2 may be somewhat closer than the others to the values that would be measured at ultra-low temperatures.

In addition to Eq. (1),

$$B_{c2} = B_0'(1-t^2)(1+t) \qquad (2)$$

is plotted in Figs. 2–5. This was obtained from Ginzburg-Landau theory using the BCS expression for the penetration depth λ.[10]

A second feature in the temperature dependence of B_{c2}, is that irrespective of where the fits are made, the low-temperature critical-field values exceed those predicted for bulk type-II superconductors. This indicates that the slopes of the critical-field boundaries are larger in layer compounds than those predicted by the theories for bulk superconductors. (This point will be elaborated upon later.) Similar results were found by Foner and McNiff[12] for $B_{c2\parallel}$ in $NbSe_2$.

B. Critical-field anisotropy $B_{c2}(\theta)$

Plots of $B_{c2}(\theta)$ vs θ at 4.2°K for $Cs_{0.3}MoS_2$ are shown in Fig. 6 and for Na_xMoS_2 at 1.17 and 2.2°K in Fig. 7. These compounds are representative of the two groups mentioned earlier. In order to compare the data with an independent-layers model and with a coupled-layers model, (both models are discussed in Sec. IV) special effort was made to take accurate data in the low-angle region $\theta \lesssim 20°$. Predictions of the two theories are also shown in Figs. 6 and 7. The critical-field anisotropies for $Cs_{0.3}MoS_2$, as well as for other compounds, are given in Table II for $t = 0$ and in Table III for $t = 0.6$.

IV. DISCUSSION

A. Temperature dependence of B_{c2}

The PC observed in the temperature dependence of B_{c2} at low fields near T_c is an unusual feature of the critical properties of the layer compounds. An examination of critical-field data on layered compounds studied by other authors [i.e., $NbSe_2$,[12,13] TaS_1Se_1,[8] and[2] $TaS_2(C_5H_5N)_{1/2}$] reveals PC in all cases, although the effect went unnoted in all but one instance.[13]

The possibility that the PC is related to a smearing of the transition caused by the inhomogeneity of the intercalated ions must be considered. However, evidence indicating that the PC is an intrinsic effect is strong: (a) PC has been observed in well-ordered crystals of $NbSe_2$ where the possibility of an inhomogeneously intercalated ion distribution does not exist. (b) The crystals of K, Rb, and $CsMoS_2$ are well ordered compounds, so PC is not due to poor crystal formation. (c) We used an inductive frequency of 100 kHz; Gamble *et al.*[2] used 17 Hz; Muto *et al.*[13] used dc resistance; and Morris and Coleman[8] used dc resistance. Thus, the effect is not peculiar to the measuring frequency or technique. (d) Limits of error for $B_{c2\parallel}$ are small enough for all samples that positive curvature is definitely established. For $B_{c2\perp}$, error bars would allow the possibility of no PC for Na, Sr, and $CsMoS_2$ and $NbSe_2$, but PC is definitely established for $B_{c2\perp}$ in Ca_xMoS_2. PC in $B_{c2\perp}$ is weakest for $Cs_{0.3}MoS_2$ (Fig. 5). Thus, we believe positive curvature of the critical boundary to be intrinsic to the layered superconductors.

The Ginzburg-Landau-Abrikosov-Gorkov theory[14] (valid near T_c) gives the temperature dependence of B_{c2} as

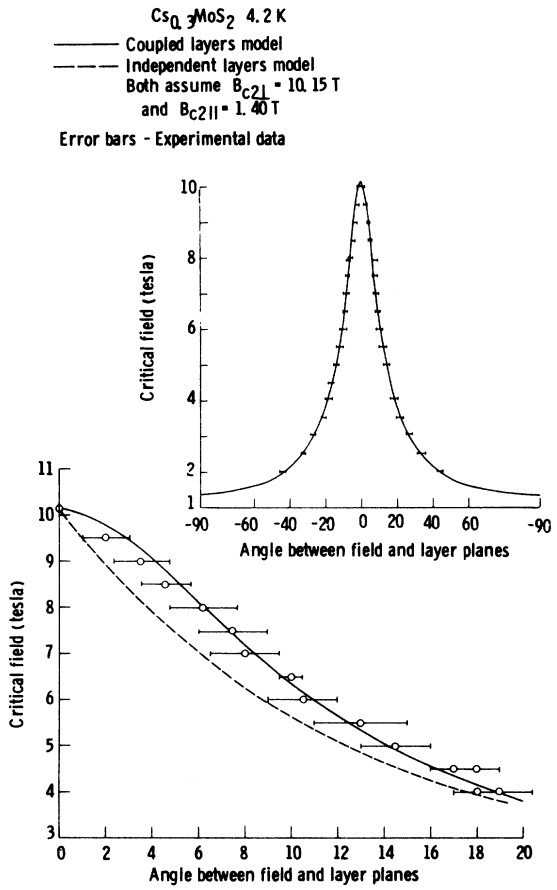

FIG. 6. Critical field vs angle between field and layer planes for $Cs_{0.3}MoS_2$ at 4.2 °K. Error bars show data taken by rotating the sample at fixed field. Critical angle is taken as the angle for onset of diamagnetism. Solid line is a plot of the coupled-layers model [Eq.(9)] and the dashed line is a plot of the independent-layers model [Eq. (12)], using $B_{c2\parallel}=10.15$ tesla and $B_{c2\perp}=1.40$ tesla. Several values of $B_{c2\perp}$ were tried to determine the best value. Inset shows the data at larger angles.

$$B_{c2}(t)=(4e/\hbar c)B_{cb}^2\lambda^2=\sqrt{2}\kappa B_{cb}(t)\,, \tag{3}$$

where $B_{cb}(t)=B_{cb}(0)\,(1-t^2)$ is the thermodynamic critical field, λ is the penetration depth, and κ is the Ginzburg-Landau parameter,

$$\kappa=\sqrt{2}(2eB_{cb}/\mu\hbar c)\lambda^2\,, \tag{4}$$

or in terms of microscopic parameters,

$$\kappa=(1/x)[0.84\lambda_L(0)](2\pi k_B T_c/\hbar v_F)\,. \tag{5}$$

In Eq. (5), $\lambda_L(0)$ is the zero-temperature London penetration depth and v_F is the Fermi velocity. For our materials, a rough calculation indicates that $\xi_0/l\sim 100$, where $\xi_0=0.18\hbar v_F/k_B T_c$ is the BCS coherence length, and l is the normal-state mean free path. Therefore, for intercalated MoS_2, the

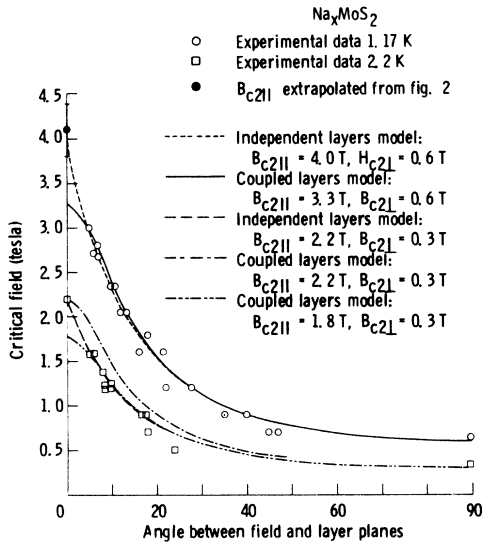

FIG. 7. B_{c2} vs angle between field and layer planes for Na_xMoS_2. Solid lines are plots of the coupled-layers model [Eq. (9)], and dashed lines are plots of the independent-layers model [Eq. (12)].

"dirty" limit ($l\ll\xi_0$) is appropriate and Eq. (5) becomes

$$\kappa_d\simeq 0.84[\lambda_L(0)/v_F](1/\tau)\,, \tag{6}$$

where the explicit dependence of κ_d on the scattering time τ is seen. All layered superconductors studied to now, including the present work, have mean free paths less than ξ, and therefore, the possible presence of positive curvature in "clean" layered superconductors has not been studied experimentally. From Eqs. (6) and (3) one finds that $B_{c2}(t)\propto B_{cb}(0)(1-t^2)$ which predicts only negative curvature.

In the Gorter-Casimir two-fluid model, the penetration depth λ is given by

$$\lambda\propto(1-t^4)^{-1/2}\,, \tag{7}$$

which from Eq. (3) gives Eq. (1),

$$B_{c2}(t)\propto(1-t^2)/(1+t^2)\,.$$

This equation is plotted in Figs. 2–5, matched to the data at $t=1$ and 0.6. Plots of Eq. (1) are omitted when the density of lines on the graph would be too great. PC is predicted by this expression but is not strong enough to fit experiment.

BCS theory for dirty superconductors gives

$$\lambda\propto(\xi_0/l)^{1/2}(1-t)^{-1/2}\,,\quad t\lesssim 1\,, \tag{8}$$

so

$$B_{c2}=B_0'(1-t^2)(1+t)\,. \tag{2}$$

This is also plotted in Figs. 2–5 (when clarity on the figures allow) and is a poorer fit to the data

than Eq. (1) given above.

Neither extensions of the Ginzburg-Landau equations to all temperatures and short mean free paths, nor the consideration of nonlocal effects can account for the PC.[15,16] Eilenberger[17] has generalized the Ginzburg-Landau equations to include anisotropic scattering and finds unusual curvatures in the critical-field behavior. The results of Eilenberger show that subtle deviations of the electronic properties from those of an isotropic electron system may alter the critical-field curvatures significantly.

Klemm, Beasley, and Luther[18,19] have calculated the temperature dependence of $B_{c2\parallel}$ for all temperatures, and various degrees of interlayer coupling. Their calculation includes results from microscopic Gorkov theory with orbital, Pauli paramagnetic, and spin-orbit scattering contributions. In their calculation, multiple electron scattering within a layer is required before tunneling to the next, and the dirty limit is assumed. Some of their results are shown in Fig. 8. τ_{so} is the spin-orbit scattering time, and α is a parameter characterizing the relative strength of pair breaking due to Pauli paramagnetism as well as orbital effects. Figure 8 demonstrates the unusual critical boundaries possible in layer compounds. The degree of the "unusualness" depends on the relative strength of the paramagnetic limiting and spin-orbit scattering. Another curve in Refs. 18 and 19 (at fixed α and τ_{so}) demonstrates the strong effect of the interlayer coupling strengths r on the critical boundary.

The physical interpretation of the Klemm *et al.* theory is that above a certain critical temperature, T^*, the coherence length, $\xi_{0\perp}$, is greater than the layer spacing and that below T^* the coherence length becomes short enough to "decouple" the layers. The very high parallel critical field for $T < T^*$ is then due to flux penetrations between the superconducting layers, since the orbital decoupling mechanism no longer exists.

Our results have two qualitative features which the Klemm-Beasley-Luther theory predicts: (i) positive curvature, as seen in Fig. 8, and (ii) upper critical fields much higher than predicted for bulk material. Not all combinations of α, τ_{so}, and r give positive curvature, but there is a wide range. If this is an applicable theory for layer superconductors, then the observation of PC in all layered superconductors to date means these samples fall in the right range of α, τ_{so}, and r. The condition of being "dirty" superconductors is easily met in all cases to date. If positive curvature is due to a transition from coupled to decoupled layers, then the coherence lengths should be comparable to the interlayer separation at t^*.

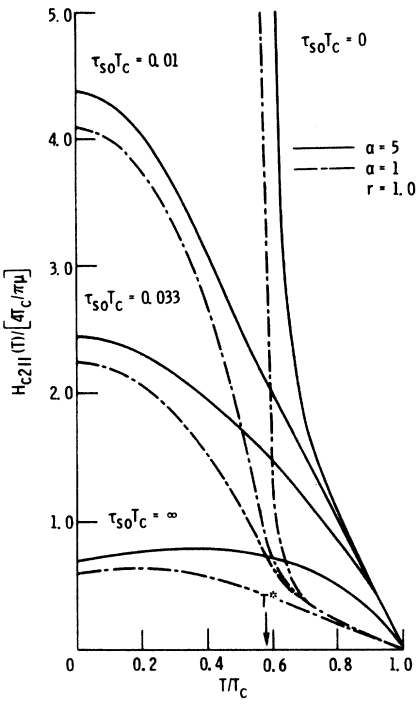

FIG. 8. Calculated reduced critical field vs reduced critical temperature for various amounts of spin-orbit scattering times, τ_{so}, and pair breaking parameter α. r is an interlayer coupling parameter (from Klemm *et al.*, Ref. 18).

Listed in Table III are estimates of $\xi_\perp$ from the coupled-layers model (to be discussed in Sec. IV C). After correcting the values listed (for $t = 0.6$), to values at t^* (estimated in Table II), it is seen that experimental $\xi_\perp$ values are a factor of 1.2 to 5 greater than interlayer separations. Another way of checking the applicability of the decoupling model for our experiments is to calculate the parameter r of the theory. The values obtained are an order of magnitude or more too large. Klemm has suggested that it may be necessary to incorporate details of the band structure into the theory. The Klemm *et al.* theory is considered again in Sec. IV D, when we discuss the paramagnetic limiting and spin-orbit scattering in more detail.

In similar calculations, Bulaevskii,[20,21] and Bulaevskii and Guseynov[22] have calculated the shape of the B_{c2} vs T_c boundary and also find PC. Their calculations also include the case of clean superconductors. Their predicted angular dependence, $B_{c2}(\theta)$, at fixed field, does not fit our data for $Cs_{0.3}MoS_2$ or Na_xMoS_2.

Positive curvature of the critical boundary was also found theoretically by Boccara, Carton, and Sarma[23] using the Ginzburg-Landau equations

TABLE III. Values of the coherence lengths and the effective masses, assuming the coupled-layer model (arbitrarily evaluated at $t=0.6$). $\xi_{\parallel}$ and $\xi_{\perp}$ come from Eq. (10) and (11) and experimental $B_{c2\parallel}$ and $B_{c2\perp}$ values. $(\xi_{\parallel}/\xi_{\perp})^2=(B_{c2\parallel}/B_{c2\perp})^2=(1/\epsilon)^2=m_{\perp}/m_{\parallel}$.

Compound	Coherence length (Å) $\xi_{\perp}$	$\xi_{\parallel}$	Critical field $B_{c2\parallel}$	$B_{c2\perp}$	$B_{c2\parallel}/B_{c2\perp}$	$m_{\perp}/m_{\parallel}$
Na_xMoS_2 ($T_c=2.2$ K)	45	320	$2.3T$	$0.32T$	7.28	53
Ca_xMoS_2 ($T_c=2.4$ K)	66	390	1.30	0.21	6.19	38
Sr_xMoS_2 ($T_c=3.36$ K)	73	230	2.00	0.63	3.17	10.1
$Cs_{0.3}MoS_2$ ($T_c=6.9$ K)	24	140	9.45	1.60	5.90	35
$NbSe_2$ ($T_c=7.3$ K)	38	120	6.8	2.10	3.2	10.5

appropriate for Josephson coupled layers, and for high fields. Their calculation is similar to one made by Klemm, Beasley, and Luther[18]; and both predict PC and an infinite critical field in the absence of paramagnetic limiting. Boccara *et al.* also find that $B_{c1\parallel}$ vs T_c has positive curvature and an inflection point. To our knowledge, the shape of B_{c1} vs T_c in layered superconductors has not been investigated.

B. Band structure and Fermi-surface anisotropy

The band structures of MoS_2 and $NbSe_2$ are quite similar[24,25] and reveal that strong intralayer hybridization between the metal d_{z^2} and d_{xy}, $d_{x^2y^2}$ bands open up a gap of 1 eV within the d manifold. The lowest d subband is filled in MoS_2, while in $NbSe_2$ it is half-filled. Upon intercalation, the electron charge donated from the alkali metal to MoS_2 raises the Fermi level from a region of extremely low density of states to one of high density. This is believed to be the major reason for the superconductivity with T_c up to 7°K in the hexagonal intercalates.

The Fermi surface of $NbSe_2$,[24,25] is calculated to consist of several separate, open and closed, cylindrical hole-type sheets, exhibiting considerable anisotropy. Additional evidence for highly anisotropic electronic properties and Fermi surface comes from the recent observation of charge density waves in TaS_2.[26] The charge density wave is due to the presence of large regions of essentially parallel sections of Fermi surface and therefore, are more probably in quasi-one- and two-dimensional systems. Similarly, considerable anisotropy should be associated with the occupied upper d bands of intercalated MoS_2.

Finally, the possibility should be considered that the intercalation of the alkali or alkaline-earth ions in the MoS_2 layers might act as a source of interlayer coupling, thereby reducing the anisotropy. We believe that the increase in interlayer separation upon intercalation of K, Rb, and Cs counteracts this possible coupling, thereby increasing rather than decreasing the anisotropy.

The anisotropic nature of the electron-phonon interaction in layered structures has been discussed by several authors.[27,28] Wieting and Verble[28] have measured the ir and Raman spectrum of MoS_2 and find that the layers are held together by interlayer forces which are approximately 100 times weaker than the intralayer forces. The magnitude of the electron-phonon-interaction anisotropy at low temperatures, or after intercalation is unknown, but certainly its anisotropic nature will still be present.

C. Critical-field anisotropy, $B_{c2}(\theta)$

The upper critical field in A_xMoS_2 is quite anisotropic (Figs. 6 and 7), as is to be expected in view of the substantial structural and Fermi-surface anisotropy of these materials. The effects of an anisotropic Fermi surface on $B_{c2}(\theta)$ may be considered theoretically, for the case where the order parameter varies slowly on the scale of interlayer separation, by substituting an effective mass tensor m_{ij} in place of the isotropic free electron mass in the Ginzburg-Landau equations.[14,29] The "effective mass approximation" has been used to calculate the critical-field anisotropy in layered structures[30,31] at $T=0$°K, and has had considerable use in the interpretation of experimental data.[7-9] This theory gives the critical-field anisotropy as

$$B_{c2}^2(\theta)=B_{c2}^2(\theta=90)/(\sin^2\theta+\epsilon^2\cos^2\theta), \tag{9}$$

where

$$B_{c2}(\theta=90)=B_{c2\perp}, \tag{10}$$

and $\phi_0 = hc/2e$. The constant ϵ^2 is the ratio of the effective masses parallel and perpendicular to the layers:

$$\epsilon^2 = m_{\parallel}/m_{\perp} = \xi_{\perp}^2/\xi_{\parallel}^2 = B_{c2\perp}^2/B_{c2\parallel}^2 \quad (11)$$

and $\xi_{\parallel}$ and $\xi_{\perp}$ are the coherence lengths parallel and perpendicular to the layers, respectively. This theory is valid only for coherence lengths greater than several layer spacings and is essentially a three-dimensional, coupled-layers model.

Another theory for critical-field anisotropy exists which is quite different from the effective mass model, and yet, can account for much of the experimental data. This theory was developed by Tinkham[32] and applied to the critical-field properties of thin type-I or -II superconductors. Use of this theory for layer compounds is justified for the case of weak interlayer coupling and temperatures not too close to T_c. Tinkham showed that for sufficiently thin films [$d \ll \xi(t)$], the critical-field anisotropy was given by

$$[B_{c2}(\theta)\cos\theta/B_{c2\parallel}]^2 + B_{c2}(\theta)\sin\theta/B_{c2\perp} = 1 . \quad (12)$$

This theory may be applied to the layered superconductors if one assumes that each layer is independent (uncoupled) from its neighbor. (Our samples are several tenths of a millimeter thick, which is much greater than ξ, so the macroscopic samples are not acting like films.) An important feature is that the angular dependences of B_{c2} given by Eqs. (9) and (12) are practically identical, within experimental error, over most of the range of θ. In the low-angle region ($0 < \theta < 20°$) the two models can best be distinguished, as can be seen by computer plots of Eqs. (9) and (12) (not shown here). The similarity of these models is due to the large anisotropy (i.e., $B_{c2\parallel} \gg B_{c2\perp}$) found in these materials. One must be cautious in arbitrarily using an effective mass model to fit angular data, and if possible, obtain data in the important angular range $0 < \theta < 20°$. Values of the effective mass ratio and the coherence lengths obtained from Eqs. (9)–(11) are given in Table III including data for $NbSe_2$ at 4.2°K.[12] All of the data in Table III correspond to approximately the same reduced temperature, $t \simeq 0.6$.

Several important features of the B_{c2} vs θ data should be mentioned. In the temperature range of the PC, where the coherence lengths are large and the coupled-layers model should be valid, neither the coupled layers [Eq. (9)] nor the independent layers [Eq. (12)] model fit the angular data. Secondly, both models predict a temperature-*independent* critical-field anisotropy, $B_{c2\parallel}/B_{c2\perp}$, which is not found experimentally in the PC temperature region, but only at lower temperatures (inset in Figs. 2–5). Thus, the appearance of PC and the breakdown of the two models in a temperature region where the coupled-layers model, at least, should be applicable, occur simultaneously, and may be related.

Also of significance is that at lower temperatures the angular dependence of $B_{c2}(\theta)$ of $Cs_{0.3}MoS_2$, which has a hexagonal structure, follows the coupled-layers model, while tetragonal Na_xMoS_2 follows an independent-layers model. It appears that the crystal-structure change upon intercalation has decoupled the interlayer Josephson tunneling in the Na_xMoS_2 case. Yet, the Na ionic diameter (in single valent chemical combination) is more than 50% smaller than that for monovalent Cs ions (Table I).

D. Paramagnetic limiting and spin-orbit coupling

At low temperatures, the value of $B_{c2\parallel}$ exceeds not only that predicted for a "dirty" or clean type-II superconductor, but also the Pauli paramagnetic limiting field $B_p = 1.84\ T_c$ (see Table II), for the hexagonal layer compounds (including K, Rb, and Cs intercalates of MoS_2 as well as the Nb and Ta compounds). The suppression of the Pauli paramagnetic effect is usually due to large spin-orbit scattering associated with a heavy atom. In our case, the spin-orbit scattering may be visualized as arising from the interaction of an electron, donated by a low atomic number (Z) impurity (the alkali metal), with a high Z matrix (i.e., MoS_2). The effect of spin-orbit scattering on the band structure of intercalated MoS_2 would be to remove the degeneracy between various sheets of the Fermi surface in the central plane of the hexagonal Brillouin zone.[24] This, in turn, could modify the Fermi-surface anisotropy.

Recently, Aoi *et al.*[33] have shown that a partially depaired superconducting state (PDS) results in the low-temperature critical fields parallel to the layers exceeding the Pauli limit by an amount which depends sensitively on the shape of the Fermi surface. The enhancement is small for spherical Fermi surfaces, but quite large for anisotropic surfaces consisting of regions of parallel (flat) pieces. As mentioned above, there is ample evidence for this type of Fermi surface in intercalated MoS_2. The conditions necessary to achieve a stable PDS state requires a small spin-orbit scattering rate, and hence, is mutually exclusive with the spin-orbit mechanism for suppression of the Pauli paramagnetic effect. The treatment by Aoi *et al.* assumes that the effect of the field on the electron motion could be neglected since the effective mass is very anisotropic ($m_{\perp}/m_{\parallel} \sim 400$) in some layered superconductors.

However, in intercalated MoS_2, this constraint is not as strong (Table III) and may adversely affect the PDS. Thus, spin-orbit scattering may be the more likely mechanism for suppression of Pauli paramagnetism in A_xMoS_2.

The Klemm-Beasley-Luther[18] calculation of the temperature dependence of $B_{c2\parallel}$ for all temperatures shows that without paramagnetic limiting $B_{c2\parallel}$ can diverge to infinity at low temperatures. With paramagnetism and spin-orbit scattering, various dependences of $B_{c2\parallel}$ on t can be found. The unusual temperature dependencies calculated for B_{c2} (Fig. 9, for example) include critical fields greatly in excess of the paramagnetic limit, depending on the relative interlayer coupling, spin-orbit scattering, and Pauli paramagnetism strengths. The biggest effects on the upper critical field come from τ_{so} and r changes. For strong interlayer coupling (larger r) the results are similar to ordinary Type-II results. The most unusual curves are for intermediate to weak coupling ($r \sim 1$). For our samples the coupling is probably intermediate to strong.

In summary, Klemm *et al.*,[18] Boccara *et al.*,[23] Bulaevskii,[20,21] and Aoi[33] have considered mechanisms which reduce paramagnetic limiting, and allow critical magnetic fields well in excess of the paramagnetic limiting field. We believe spin-orbit scattering is more likely than the PDS to be the origin of high critical fields in A_xMoS_2.

E. General trends throughout the series of intercalates

One of the purposes of studying the alkali and alkaline-earth series of intercalates of MoS_2 was to look for systematic trends in the superconducting properties as a function of parameters such as the crystal structure, the ionic radii, or the ionization potential of the intercalate. We find that the transition temperature increases with increasing ionic diameter of the intercalate, or alternatively, with increasing crystal symmetry (Table I). Within the K, Rb, and Cs intercalate series, which maintain the hexagonal structure, experimental errors mask any possible trends, but T_c is significantly higher for this group than for the nonhexagonal Na, Ca, Sr group (Table II). These two groups can be separated by other properties also (Table II), such as critical boundary slopes, $dB_{c2\parallel}/dT_c$, as can be seen by plotting the ionic radii vs T_c slope. Examination of Table II also reveals that all the hexagonal structure materials [including K, Rb, and Cs intercalates as well as $NbSe_2$, $TaS_2(C_5H_5N)_{1/2}$, and TaS_1Se_1] have $B_{c2\parallel}(0)$ greater than the paramagnetic limiting fields, and the nonhexagonal structures have $B_{c2\parallel}(0) \ll B_p$. These differences may result from the higher structural anisotropy of the hexagonal group, yet, it is puzzling why the groupings are not reflected in $B_{c2\parallel}/B_{c2\perp}$. It appears then, that the superconducting critical properties are dominated by the crystal structure, and thus the structural anisotropy. Information on the bonding strength anisotropy in the intercalation compounds (from Raman scattering, for example) would be very helpful.

V. CONCLUSIONS

The critical-field anisotropy and temperature dependence in the alkali and alkaline-earth intercalates of MoS_2 have been measured. An unusual positive curvature in the critical-field–temperature boundary at high temperatures and low fields has been observed. This curvature has also been found in all layered superconductors for which data are available, and therefore, appears to be a universal feature of layered superconductors. Possible theoretical explanations for this behavior have been discussed.

In the temperature region where the PC is observed, neither a coupled-layers model nor an independent-layers model can account for the data. The low-temperature critical-field anisotropy $B_{c2}(\theta)$ can be explained by the independent-layers model for Na_xMoS_2, and by the coupled-layers model for $Cs_{0.3}MoS_2$. If the coupled-layers model is assumed, then mass anisotropies range from 10 to 50 with no obvious systematic trend through the Periodic Table.

The alkali and alkaline-earth series have two groupings of properties. The materials with the largest ionic intercalate atom diameters and hexagonal crystal structures (K, Rb, and Cs compounds) have the highest critical temperatures, critical fields, and critical boundary slopes. For all cases in this group, including the niobium and tantalum compounds, the hexagonal materials have critical fields exceeding the paramagnetic limiting field. The angular dependence of B_{c2} follows a coupled layers model for $Cs_{0.3}MoS_2$ which may be representative of this group, since all the $B_{c2\parallel}$ and $B_{c2\perp}$ critical data are similar for this group. The second group consists of the Na, Sr, and Ca intercalates of MoS_2 where structures are not hexagonal, and critical temperatures, critical fields, and critical boundary slopes are small compared to those for the hexagonal structure group, and the paramagnetic limit is not exceeded.

ACKNOWLEDGMENTS

Several people have contributed to this work at various stages. These include David Wagoner, Dennis Flood, Paul O'Connor, Jerry Kraynik, and Lynne Talley at NASA Lewis; Stan Samson, Vaclav Hadek, and Alan Rembaum at the Jet Propulsion Laboratory. The Jet Propulsion Lab part of this research was sponsored by NASA Contract No. NAS7-100.

[1]J. A. Wilson and A. D. Yoffe, Adv. Phys. 18, 193 (1969).
[2]F. R. Gamble, F. J. DiSalvo, R. A. Klemm, and T. H. Geballe, Science 168, 568 (1970).
[3]R. B. Somoano and A. Rembaum, Phys. Rev. Lett. 27, 402 (1971).
[4]R. B. Somoano, V. Hadek, and A. Rembaum, J. Chem. Phys. 58, 697 (1973).
[5]A. M. Hermann, R. B. Somoano, V. Hadek, and A. Rembaum, Solid State Commun. 13, 1065 (1973).
[6]R. B. Somoano, V. Hadek, A. Rembaum, S. Samson, and J. A. Woollam, J. Chem. Phys. 62, 1068 (1975).
[7]R. C. Morris, R. V. Coleman, and R. Bhandari, Phys. Rev. B 5, 895 (1972).
[8]R. C. Morris and R. V. Coleman, Phys. Rev. B 7, 991 (1973).
[9]P. deTrey, S. Gygax, and J. P. Jan, J. Low Temp. Phys. 11, 421 (1973).
[10]J. A. Woollam, R. B. Somoano, and P. O'Connor, Phys. Rev. Lett. 32, 712 (1974).
[11]A. L. Schawlow and G. E. Devlin, Phys. Rev. 113, 120 (1959).
[12]S. Foner and E. J. McNiff, Jr., Phys. Lett. A 45, 429 (1973).
[13]Y. Muto, N. Toyota, K. Noto, and A. Hoshi, Phys. Lett. A 45, 99 (1973). These authors recognized the positive curvature in $NbSe_2$.
[14]N. R. Werthamer, in *Superconductivity*, edited by R. D. Parks (Marcel Dekker, New York, 1969), p. 321.
[15]K. Maki, Physics 1, 21 (1964).
[16]P. C. Hohenberger and N. R. Werthamer, Phys. Rev. 153, 493 (1967).
[17]G. Eilenberger, Phys. Rev. 153, 584 (1967).
[18]R. A. Klemm, M. R. Beasley, and A. Luther, J. Low Temp. Phys. 16, 607 (1975).
[19]R. A. Klemm, Ph. D. thesis (Harvard University, 1974). (unpublished).
[20]L. N. Bulaevskii, Zh. Eksp. Teor. Fiz. 64, 2241 (1973) [Sov. Phys.-JETP 37, 1133 (1973)].
[21]L. N. Bulaevskii, Zh. Eksp. Teor. Fiz. 65, 1278 (1973) [Sov. Phys.-JETP 38, 634 (1974)].
[22]L. N. Bulaevskii, and A. A. Guseynov, Zh. Eksp. Teor. Fiz. Pis'ma Red. 19, 742 (1974) [JETP Lett. 19, 382 (1974)].
[23]N. Boccara, J. P. Carton, and G. Sarma, Phys. Lett. A 49, 165 (1974).
[24]L. F. Mattheiss, Phys. Rev. B 8, 3719 (1973). (References to previous band-structure calculations contained within.)
[25]R. A. Bromley, Phys. Rev. Lett. 29, 357 (1972).
[26]J. A. Wilson, F. J. DiSalvo, and S. Mahajan, Phys. Rev. Lett. 32, 882 (1974).
[27]R. Fivaz and E. Mooser, Phys. Rev. 163, 743 (1967); 136, A833 (1964).
[28]J. L. Verble and T. J. Wieting, Solid State Commun. 11, 941 (1972), and references therein.
[29]D. R. Tilley, Proc. Phys. Soc. Lond. 86, 289 (1965).
[30]E. I. Kats, Zh. Eksp. Teor. Fiz. 56, 1675 (1969)[Sov. Phy.-JETP 29, 897 (1969)].
[31]W. E. Lawrence and S. Doniach, *in Proceedings of International Conference on Low-Temperature Physics, 1970* (Academic Press of Japan, Tokyo, 1970), Vol. 12, p. 361.
[32]M. Tinkham, Phys. Rev. 129, 2413 (1963).
[33]K. Aoi, W. Dieterich, and P. Fulde, Z. Phys. 267, 223 (1974).